Ionic contraction across the lanthanide series decreases the temperature-induced disorder of the water coordination sphere

Darren M. Driscoll[2, #, &], Richard C. Shiery[1, #], Mahalingam Balasubramanian[2, ^], John L. Fulton[3], David C. Cantu[1, *]

[1]*Department of Chemical and Materials Engineering, University of Nevada, Reno, Reno, NV 89557, USA*

[2]*Advanced Photon Source, Argonne National Laboratory, Lemont, IL 60439, USA*

[3]*Physical Sciences Division, Pacific Northwest National Laboratory, Richland, WA 99352, USA*

[*]Corresponding author: dcantu@unr.edu

[#]Equal contribution

[&] Present Address: Chemical Sciences Division, Oak Ridge National Laboratory, Oak Ridge, TN 37831, USA

[^] Present Address: Electrification and Energy Infrastructures Division, Oak Ridge National Laboratory, Oak Ridge, TN 37831, USA

ABSTRACT

In liquid, temperature affects the structures of lanthanide complexes in multiple ways that depend upon complex interactions between ligands, anions, and solvent molecules. The relative simplicity of lanthanide aqua ions (Ln^{3+}) make them well suited to determine how temperature induces structural changes in lanthanide complexes. We performed a combination of ab initio molecular dynamics (AIMD) simulations and extended X-ray absorption fine structure (EXAFS) measurements, both at 25 °C and 90 °C, to determine how temperature affects the first- and second-coordination spheres of three Ln^{3+} (Ce^{3+}, Sm^{3+}, Lu^{3+}) aqua ions. AIMD simulations show first lanthanide coordination spheres that are similar at 25 °C and 90 °C; more so for the Lu^{3+} ion that remains eight-coordinate, than for the Ce^{3+} and Sm^{3+} ions that change their preferred coordination number from nine (at 25 °C) to eight (at 90 °C). The measured EXAFS spectra are very similar at 25 °C and 90 °C, for the Ce^{3+}, Sm^{3+}, and Lu^{3+} ions, suggesting that the dynamical disorder of the Ln^{3+} ions in liquid water is sufficient such that temperature induced changes do not clearly manifest changes in the structure of the three ions. Both AIMD simulations and EXAFS measurements show very similar structures of first coordination sphere of the Lu^{3+} ion at 25 °C and 90 °C.

1. Introduction

Probing the structure of aqueous lanthanide (Ln) ions with changes in temperature provides key insights into the factors controlling various first coordination sphere structures. Since the Ln properties of interest (e.g., ligand binding strength, luminescence, coordination, catalytic rates) depend on molecular structure, resolving if and how temperature changes Ln-containing structures is important to determine how these fundamental properties will be affected. For example it has been shown that i) the stability constants of Ln-ligand complexes change with temperature,[1] the intensity of emission spectra of Ln-ligand complexes show significant changes with temperature;[2] iii) the Ln coordination structure in peptides is flexible, sensitive and changes for different Ln^{3+} ions;[3] and iv) the structure of Ln-ligand catalysts affects redox reactions.[4] The associated applications will likely also be impacted or controlled by temperature-induced structural changes, including i) separations in which temperature affects Ln extraction;[5,6] ii) non-invasive nanothermometers, where it is desirable to have Ln-ligand complexes with highly temperature-sensitive dependence of their luminescent properties;[7,8] iii) synthetic peptides for Ln^{3+} binding, which could change binding affinity to a particular Ln^{3+} ion with temperature, and iv) Ln homogeneous catalysts reaction rates, which may vary according to changes in the catalyst structure due to temperature.

Temperature affects Ln-ligand structures in different ways that depends upon complex interactions between different ligands, anions, and solvent molecules. For this reason, the relative simplicity of aqua Ln^{3+} ions make them well suited to assess the structural changes of these cations with temperature. Here we describe how temperature changes the first- and second-coordination spheres about Ce^{3+}, Sm^{3+}, and Lu^{3+} aqua ions that were selected from the center and the two endpoints of the Ln series.

Computationally, the coordination structures of the Ln aqua ions have been studied with electronic structure calculations,[9–11] ab initio molecular dynamics simulations,[12–15] and classical molecular dynamics simulations.[16–30] Experimentally, their structures have been resolved with X-ray diffraction,[31–33] X-ray absorption spectroscopy,[34–38] and excitation and emission spectroscopy.[39] Most computational and experimental studies on the structure of Ln aqua ions have been done at room temperature, although the temperature dependence of water exchange rates has been investigated with classical molecular dynamics.[18] There are studies that report the structure of Ln aqua ions in different phases: between liquid and frozen water,[39] crystal and

solution phases,[38] hydrated in liquid water and solidified with ligands,[36] and water liquid and glassy states.[34] In this work, we focus on the effect of temperature on the coordination structure of Ln ions in liquid water.

Temperature dependent extended X-ray absorption fine structure (EXAFS) measurements of ions have been employed extensively to describe atomic structure within solutions.[40,41] Temperature induced structural transitions in both geometry and coordination have been shown to occur in a variety of metal ion-based solutions.[42–44] These solvation and structural transitions can be captured and quantified through element-specific EXAFS measurements. Specifically, EXAFS is highly sensitive to changes in bond lengths, solvation geometry and speciation through analysis of the photoelectron scattering paths.

This work reports a combination of ab initio molecular dynamics (AIMD) simulations, EXAFS measurements, and predicted EXAFS spectra from AIMD simulations, that were used to determine how temperature affects the structure of the first and second coordination spheres of the Ce^{3+}, Sm^{3+}, and Lu^{3+} ions in liquid water.

2. Methods

2.1. Ab initio molecular dynamics simulations

Previously we simulated all Ln^{3+} aqua ions in water, at 25 °C, using density functional theory (DFT) level AIMD simulations: predicted Ln-O distances are within ~0.05 Å from those measured with EXAFS.[12] In this work, we took room-temperature equilibrated frames from the Ce^{3+}, Sm^{3+}, and Lu^{3+} trajectories and ran AIMD simulations at 90 °C to determine how temperature affects the structure of their first coordination spheres.

DFT-level AIMD simulations were done in the PBE functional[45] using the CP2K package[46,47]. Core electrons were modeled with norm-conserving GTH pseudopotentials[48], valence electrons were modelled with polarizable double-zeta basis sets[49], and our LnPP1 pseudopotentials and basis sets[50] were used for Ce^{3+}, Sm^{3+}, and Lu^{3+}. Long range electrostatic terms were determined with a supplementary plane wave basis set,[51] using a 500 Ry cutoff for Ce and Sm, and 1000 Ry Lu. Grimme's D3 corrections[52] were used to account for van der Waals

interactions within a 6.0 Å radius in all simulations. Ln Multiplicities were assigned with Hund's rule, see **Table S1** of the Supporting Information (SI).

AIMD simulations were done in periodic boundary conditions with cubic boxes having a length of 12.42 Å, with 64 explicit water molecules, which corresponds to a density of 0.998 g/mL. Three Cl^- anions were added to neutralize the charge of the Ln^{3+} cations. AIMD simulations were done in the canonical (NVT) ensemble at 90 °C with 1 fs time steps. The simulations were performed until at least 10 ps of simulation with a stable potential (SI, **Figures S1 – S3**) were observed, which were used to calculate Ln-O radial distribution functions (RDFs), O-Ln-O angle distribution functions (ADFs), calculate root mean square distances (RMSDs) to ideal geometries, and to predict EXAFS spectra.

2.2. Predicted extended X-ray absorption fine structure spectra

The EXAFS photoelectron single-scattering process provides a simple and accurate measure of the first-shell Ln-O distances. EXAFS spectra can be predicted from molecular dynamics simulations.[53] Comparing predicted and measured EXAFS spectra has been done to determine the coordination structure of heavy elements[12,54]. To directly compare with measured EXAFS spectra, we predicted $\chi(k)$ spectra from AIMD trajectories[55], using FEFF8.5[56]. The Ln and O coordinates from 200 equispaced frames from equilibrated AIMD trajectories were used to generate ensemble average spectra. An AIMD-EXAFS spectrum[53,55,57] is generated for each frame and ensemble-average spectra resulted from the 200 frames of each case. FEFF8.5 was adjusted to include up to 35,000 paths. Only Ln and O atoms were included in FEFF calculations because the inclusion of H atoms results in a large number of scattering paths that fail to converge. The Hedin-Lundqvist exchange-correlation potential (default for FEFF8.5) was used with no SCF.

2.3. Measured extended X-ray absorption fine structure spectra

X-ray absorption spectroscopic measurements were performed on the L_3-edge of aqueous Ln (Ce^{3+}, Sm^{3+}, and Lu^{3+}) solutions at 20-BM of the Advance Photon Source. Ln(III) triflate salts (Alfa Aesar) were added to 0.1 M triflic acid to generate solutions containing 0.1 M of the Ln^{3+} species. These solutions are expected to be fully dissociated in aqueous environments and therefore effectively interrogate the Ln^{3+}-aqueous solvation structure, and were compared with

analogous experiments in which Ln(III)nitrate was used as the starting material, see Figure S4 in the SI). Solutions were deposited into PEEK liquid cell holders with Kapton windows sealed with epoxy. A Si(111) monochromator with harmonic rejection set to 11 KeV was used. The beam was detuned 15% at 7 keV. Spectra were acquired in transmission mode with ionization gas chambers before (50 % N_2, 50 % He) and after (100% N_2) the sample. Energy calibration was achieved by periodic measurement of an Fe foil. XAS measurements at elevated temperatures were performed under the same beamline settings utilizing a resistively-heated sample holder which uses a Lakeshore controller. For high temperature measurements (90°C), the sample holder was heated at an approximate rate of 5 °C per minute and held at the desired temperature for an additional 20 minutes to allow for equilibration of the sample. XAS analysis was performed in the Athena software package.[58] Briefly, the absorption edge for each sample was normalized to unit step height and the extraction of the $\chi(k)$ was performed through the use of a spline function with a cutoff distance (R_{BKG}) of 1.2 Å.

3. Results

Figure 1 includes the radial distribution functions (RDFs) from the AIMD simulations of the Ce^{3+}, Sm^{3+}, and Lu^{3+} aqua ions, at 25 °C and 90 °C. As expected, the increase in temperature resulted in shorter, broader peaks in the oxygen – oxygen RDFs in all cases (**Figure 1**, RHS). However, temperature had a much less pronounced effect on Ln-O RDFs (**Figure 1**, LHS). The first peak of Ce- and Sm-O distances shows slightly lower Ln-O distances at 90 °C than at 25 °C, which is counterintuitive. This can be explained by the fact that the Ce^{3+} and Sm^{3+} aqua ions changed their coordination number: they are 9-coordinate in the 25 °C AIMD simulations but 8-coordinate in the 90 °C AIMD simulations. The rearrangement of the second coordination sphere due to the change in coordination number in the first sphere also explains why temperature seemingly does not change the second peak in the Ce- and Sm-O RDFs: in simulation, the second sphere effects of temperature and change in coordination number average out.

On the other hand, the Lu^{3+} aqua ion remained 8-coordinate at 90 °C. This allows to isolate the effect of temperature on the structure of the first and second solvation sphere without a change in coordination number. The Lu-O RDF shows an almost identical first peak at 25 °C and 90 °C, but the second peak is broader at 90 °C than at 25 °C (**Figure 1**, LHS, bottom row).

This implies that temperature has almost no effect on the first coordination sphere of the Lu^{3+} ion, which is somewhat unexpected, but it did make the second sphere more disordered, as expected.

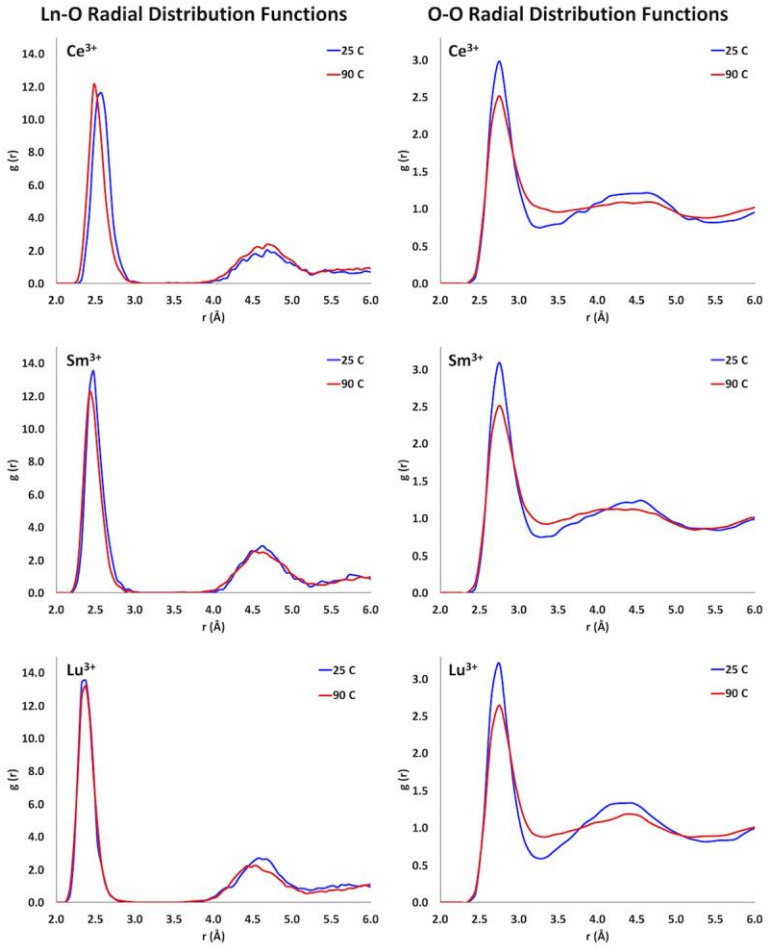

Figure 1: Plots of Ln-O (left hand column) and O-O radial distribution functions (right hand column) of the Ce^{3+} aqua ion (top row), Sm^{3+} aqua ion (middle row), and Lu^{3+} aqua ion (bottom row) AIMD simulations, each case at 25 °C (blue) and 90 °C (red).

Figures 2 and **3** compare the EXAFS $\chi(k)$, and the Fourier-transformed $\chi(R)$ spectra generated from AIMD simulations with those measured in the experiment. The $\chi(k)$ from the AIMD (**Figure 2**, LHS) show that increasing the temperature from 25 °C to 90 °C has a modest effect on the predicted spectra. The Ce $\chi(k)$ spectra in **Figure 2**, and to a lesser extent the Sm spectra, show appreciable phase shifts in the oscillations consistent with a contraction in the Ln-

O bond distance at higher temperature. It is important to note that the simulated spectra for Lu^{3+} at 25 °C and 90 °C are both from eight-coordinate first-sphere structures, while those for Ce^{3+} and Sm^{3+} represent an eight-coordinate structure at 90 °C and a nine-coordinate structure at 25°C. Thus, to a large extent the change coordination number in first sphere symmetry explains the observed differences in the AIMD EXAFS spectra of the Ce^{3+} and Sm^{3+} ions at the two different temperatures. The AIMD-predicted Lu^{3+} ion EXAFS spectra show a small but systematic shift to lower *k*-values at 90 °C, which corresponds to a slightly increased average distance of the first coordination shell, as shown in the first peak of the Lu-O RDF (**Figure 1**, LHS bottom row). In comparison, the experimental $\chi(k)$ spectra (RHS) show little or no changes with temperature. There are, however, small change in the amplitude of the experimental oscillations for all three ions, but most significantly for the Lu^{3+} ion.

The $\chi(R)$ spectra in **Figure 3** provide further insights into the difference between AIMD and experiment. The AIMD spectra for Ce^{3+} and Sm^{3+} (LHS) show a contraction of the distance and a reduction in the amplitude of the $\chi(R)$ that is consistent with the difference in the nine- (25 °C) versus the eight-coordinate (90 °C) ions. In comparison, the experimental spectra (RHS), show rather small changes. Notably the Lu^{3+} shows a slight reduction in the amplitude to a lesser extent than that for the Sm^{3+} ion, which shows a very slight contraction in the Sm-O bond. While both trends are also observed for the AIMD structures, they exhibit far lower magnitudes in the experiment. The near-identical first peak of the Lu-O RDFs at 25 °C and 90 °C (**Figure 1**, bottom row) corresponds with the near-identical EXAFS spectra for Lu^{3+} at 25 °C and 90 °C, for both measured and predicted spectra (**Figures 2** and **3**, bottom row).

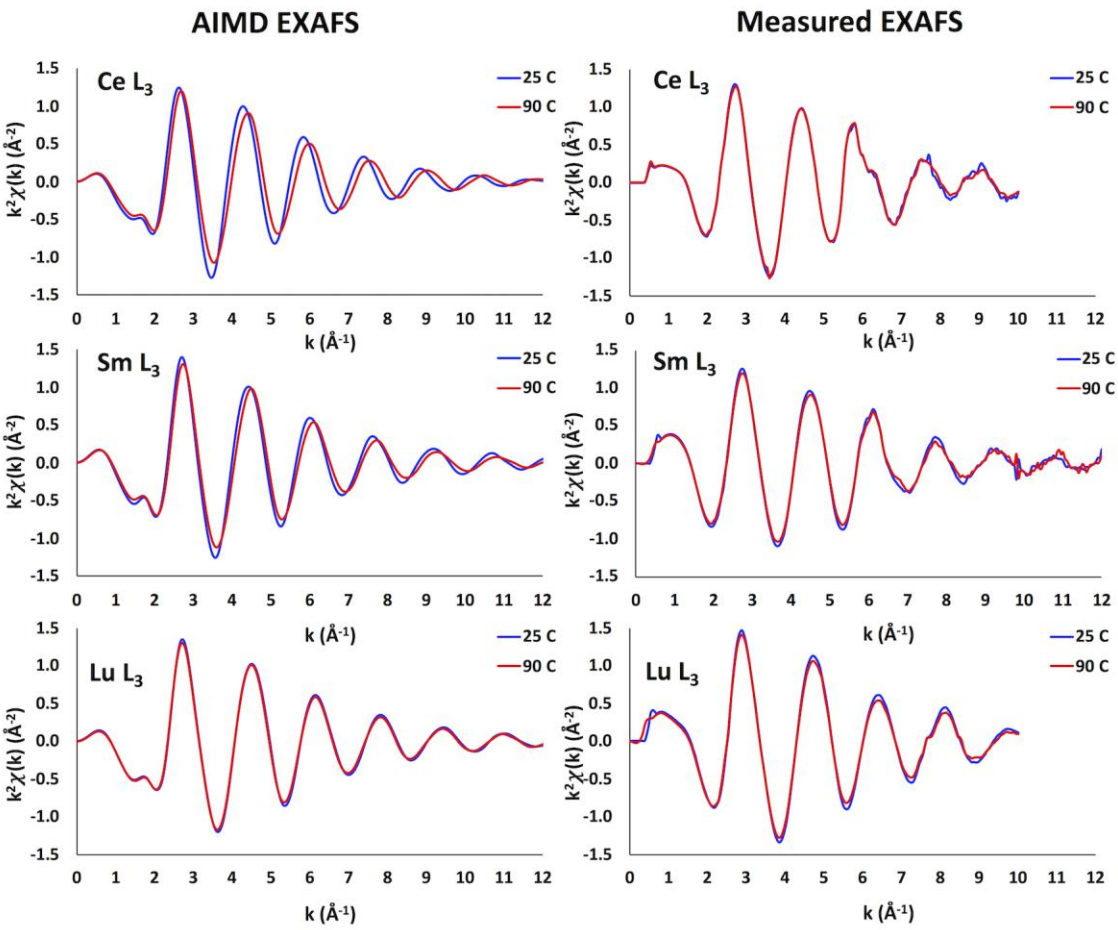

Figure 2: k^2-weighted $\chi(k)$ spectra of the Ce^{3+} (top row), Sm^{3+} (middle row), and Lu^{3+} (bottom row) L_3-edges, independently measured by experiment (right hand column) and predicted with simulation (left hand column), each case at 25 °C (blue) and 90 °C (red).

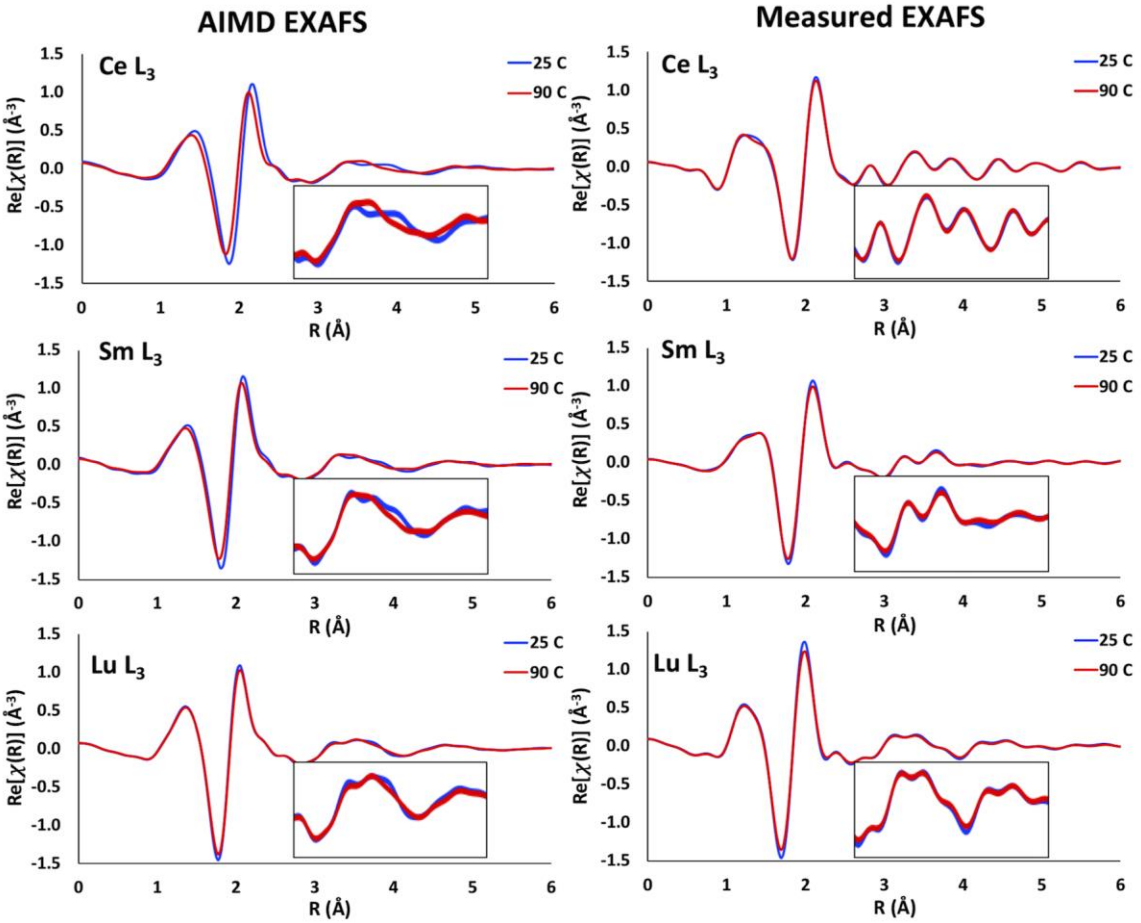

Figure 3: *Re*[$\chi(R)$] spectra derived from k^2-weighting of the Ce^{3+} (top row), Sm^{3+} (middle row), and Lu^{3+} (bottom row) L_3-edges, independently measured by experiment (right hand column) and predicted with simulation (left hand column), each case at 25 °C (blue) and 90 °C (red). The inserts of the figures show the expanded regions between 2.8 to 5 $Å^{-1}$ where the multiple scattering contributions, that are enhanced by certain symmetries, become more important.

4. Discussion

A change in the coordination number of the first sphere, or symmetry of the first sphere within a coordination number, would be detected in EXAFS as modest changes in average Ln-O distances or Debye-Waller factors. However, the multiple scattering region, from ~2.5 < R < ~6 Å, shown in the **Figure 3** inserts, provides a much more sensitive fingerprint of the coordination symmetry.[12] For the AIMD (**Figure 3** LHS inserts), the structure of the multiple scattering regions at 25 °C and 90 °C are significantly different for Ce^{3+}, and Sm^{3+} ions, and to a less but still significant extent for the Lu^{3+} ion. In contrast, the experimental spectra (**Figure 3** RHS

inserts) show very little change in this multiple scattering region. It should be noted that for the experimental Ce^{3+} spectra, the multiple scattering region is distorted to some extent by a large multi-electron excitation in the $\chi(k)$,[12,59] near 6 $Å^{-1}$, see **Figure 2**.

While the AIMD shows some changes in $\chi(R)$ spectra between 25 °C and 90 °C, the experimental results mostly do not. A possible explanation for this discrepancy between measured- and AIMD-EXAFS could be because the AIMD simulations did not sample water exchange events. The small differences between 25 °C and 90 °C experimental spectra could be due to a small change in the equilibrium between 9- and 8-coordinate species, or in the equilibrium between different symmetries within the same coordination number. Either way, there could be only small changes in the relative distribution of populations between 25 °C and 90 °C, as shown by similar experimental multiple scattering spectra (**Figure 3** RHS inserts).

This contrasts with the AIMD simulations, which treat the Ln^{3+} ions as having a single coordination number. A limitation of AIMD simulations is that nanosecond or greater timescales are not attainable, and therefore we cannot simulate water exchange events or back-and-forth changes in coordination number,[60] which results in that the AIMD simulations includes only equilibrium sampling of single coordination number conformations. Longer time scales would result in non-integer average coordination numbers that are a more complete sample of what is observed in experiment.[36] Since temperature is likely to reduce the difference in population between 9- and 8-coordinate species (these were estimated with electronic structure calculations for the Ce^{3+} aqua ion to change from ~31:1 CN=9:CN=8 species at 25 °C to ~13:1 CN=9:CN=8 species at 90 °C, see SI), longer simulation times that sample both coordination numbers could be used to accurately determine the free energy difference and relative populations of both coordination numbers at 25 and 90 °C. This likely explains why, for the Ce^{3+} and Sm^{3+} aqua ions, the AIMD EXAFS spectra (**Figures 2** and **3**, LHS) shows more differences between 25 °C and 90 °C than the measured EXAFS spectra (**Figures 2** and **3**, RHS). Longer AIMD simulations, with water exchange events, will likely result in EXAFS spectra whose differences between 25 °C and 90 °C more closely agrees with experiment.

Although AIMD simulations cannot sample water exchange events, they can identify the preferred coordination number of lanthanide aqua ions.[12] The Ce^{3+} and Sm^{3+} ions began as 9-coordinate in the AIMD simulations at 90 °C (starting point was the equilibrated 25 °C structures), however, they readily became 8-coordinate in the AIMD time scale at 90 °C,

therefore the equilibrium simulation of the Ce^{3+} and Sm^{3+} aqua ions only samples 8-coordinate conformations.

Another possibility to explain why measured-EXAFS shows smaller differences between 25 °C and 90 °C than and AIMD-EXAFS is that while the symmetry may remain the same, the occupancy of one or more of the sites is changing. For instance, for Lu^{3+}, the multiple scattering region shows little change in structure corresponding to a fixed symmetry while there is small reduction in the amplitude corresponding to a reduction in the Ln-O coordination number. We expect that changes with temperature in the geometry of Ln^{3+} aqua ions might have some influence on the X-ray absorption near edge structure, which is expected to be less sensitive to disorder than EXAFS.

The O-Ln-O angle distribution functions (**Figure 4**) from AIMD simulations, which correspond to the first peak of the Ln-O RDFs, show similar findings. For the Ce^{3+} and Sm^{3+} ions, the ADFs between 25 °C and 90 °C vary, due to the change in coordination number. For the Lu^{3+} ion, the ADFs at 25 °C and 90 °C are quite similar. A small difference is observed: the broadening of a minor peak around ~115° - 120° at the higher temperature. This is explained by the fact that, at room temperature, the Lu^{3+} aqua ion, although highly disordered and dynamical,[12] prefers the square antiprismatic geometry.[12,21] However, at 90 °C the dodecahedral geometry becomes preferred over the square antiprism. This is shown in the bottom frame of **Figure 4**, which superimposes the Lu^{3+} ion's ADFs with the angle distributions of ideal square antiprism and dodecahedral geometries. Also, the RMSD of the first coordination sphere of the Lu^{3+} aqua ion to the square antiprism slightly increased from 0.39+/-0.03 Å to 0.43+/-0.04 Å between 25 °C and 90 °C; it slightly decreased to the dodecahedral geometry from 0.44+/-0.02 Å to 0.41+/-0.05 Å; see RMSD analysis details in the SI.

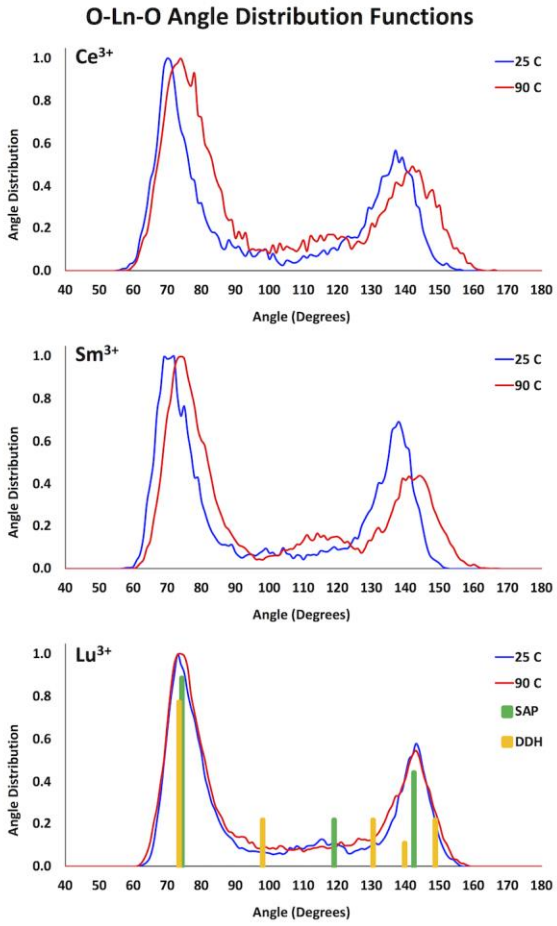

Figure 4: Plots of O-Ln-O angle distribution functions of the Ce^{3+} aqua ion (top row), Sm^{3+} aqua ion (middle row), and Lu^{3+} aqua ion (bottom row) AIMD simulations, each case at 25 °C (blue) and 90 °C (red), normalized for comparison. The angle distribution of the square antiprism (SAP, green) and dodecahedral (DDH, yellow) ideal geometries are superimposed for visual comparison.

There is distinction to be made regarding the definition of disorder for water molecules in the first coordination sphere of cations. The Debye-Waller factor (σ^2) for the Ln-O interaction in EXAFS measures only the radial component of the thermal ellipsoid of the oxygen atom with respect to the Ln position. The experimental, and simulated, Debye Waller factors for Ln^{3+} ions (~0.007 $Å^2$) are approximately the same as for first-row transition metals.[12,61] First-row transition elements, in the III oxidation state, are considered to have well-ordered first spheres water molecules with octahedral symmetry. In the case of the Ln^{3+} ions, however there may be larger disorder in the symmetry within the water hydration sphere due to water packing efficiency: an excess of ion-surface area can accommodate multiple symmetries with a higher degree of

disorder than suggested by a relatively small Debye-Waller factor. At 25 °C, the lanthanide contraction reaches a point around the middle of the series where the packing limitation favors a change in coordination number from 9 to 8. The AIMD simulations in this work suggest that at 90 °C this change occurs in the early lanthanides; therefore, the later lanthanides remain 8-coordinate 90 °C, with water molecules in the first sphere that show similar disorder at 25 °C and 90 °C.

5. Conclusions

AIMD results suggest that the first coordination sphere of the lanthanide aqua ions remain similarly disordered as temperature increases, more so for the Lu^{3+} ion that remains eight-coordinate, than for the Ce^{3+} and Sm^{3+} ions that change their preferred coordination number from nine to eight. Measured EXAFS spectra suggest that Ln^{3+} aqua ions have enough dynamical disorder in their first coordination sphere that temperature induced changes, between 25 °C and 90 °C, do not clearly manifest changes of the Ce^{3+}, Sm^{3+}, and Lu^{3+} ions structures. EXAFS measurements and AIMD simulations both point to a structure of first coordination sphere of the Lu^{3+} ion that almost does not vary between 25 °C and 90 °C. Lanthanide – water coordination bonds have a highly ionic character that allow disorder in the geometry of the first coordination sphere at room temperature, yet are strong enough that temperature does not increase their disorder significantly, aside from changing the preferred coordination number from nine to eight for the lighter- to middle-lanthanides. As the lanthanide aqua ions are contracted along the series due to *f* electrons there is less temperature-induced disorder of the first coordination sphere.

Supporting Information
Electronic configuration and multiplicities of Ln^{3+} ions; potential energy plots of 90 °C simulations; Spectra with nitrate and triflate salts; Discussion on the effect of temperature on the equilibrium between 9- and 8-coordinate Ce^{3+} ion; RMSD analysis

ORCID
Darren M. Driscoll: 0000-0001-8859-8016
Richard C. Shiery: 0000-0002-7606-1307
Mahalingam Balasubramanian: 0000-0002-3988-3125
John L. Fulton: 0000-0001-9361-9803
David C. Cantu: 0000-0001-9584-5062

Acknowledgments
The authors thank Cailin Buchanan and Nirala Singh, from the University of Michigan, for providing Ln^{3+} salt samples. R.C.S. and D.C.C. acknowledge support from the donors of the American Chemical Society Petroleum Research Fund. Work by J.L.F. was supported under project 16248, funded by the U.S. Department of Energy (DOE), Office of Science, Office of Basic Energy Sciences, Division of Chemical Sciences, Geosciences and Biosciences. Pacific Northwest National Laboratory (PNNL) is operated by Battelle for the U.S. DOE under Contract No. DE- AC05-76RL01830. This research used resources of the Advanced Photon Source, a U.S. Department of Energy (DOE) Office of Science User Facility operated for the DOE Office of Science by Argonne National Laboratory under Contract No. DE-AC02-06CH11357. Calculations were performed in Pronghorn, the High-Performance Computing cluster of the University of Nevada, Reno.

References

(1) Smith, R. M.; Martell, A. E. *Critical Stability Constants: Inorganic Complexes*; Springer, 1976; Vol. 4.
(2) Monteiro, J. H. S. K.; Sigoli, F. A.; de Bettencourt-Dias, A. A Water-Soluble TbIII Complex as a Temperature-Sensitive Luminescent Probe. *Can. J. Chem.* **2018**, *96*, 859–864.
(3) Liu, S.; Featherston, E. R.; Cotruvo, J. A.; Baiz, C. R. Lanthanide-Dependent Coordination Interactions in Lanmodulin: A 2D IR and Molecular Dynamics Simulations Study. *Phys. Chem. Chem. Phys.* **2021**, *23*, 21690–21700.
(4) Qiao, Y.; Schelter, E. J. Lanthanide Photocatalysis. *Acc. Chem. Res.* **2018**, *51*, 2926–2936.
(5) Nilsson, M.; Nash, K. L. Trans-Lanthanide Extraction Studies in the TALSPEAK System: Investigating the Effect of Acidity and Temperature. *Solvent Extr. Ion Exch.* **2009**, *27*, 354–377.
(6) Jordan, N.; Demnitz, M.; Lösch, H.; Starke, S.; Brendler, V.; Huittinen, N. Complexation of Trivalent Lanthanides (Eu) and Actinides (Cm) with Aqueous Phosphates at Elevated Temperatures. *Inorg. Chem.* **2018**, *57*, 7015–7024.
(7) Jaque, D.; Vetrone, F. Luminescence Nanothermometry. *Nanoscale* **2012**, *4*, 4301–4326.
(8) Wang, X.; Wolfbeis, O. S.; Meier, R. J. Luminescent Probes and Sensors for Temperature.

Chem. Soc. Rev. **2013**, *42*, 7834–7869.
(9) Clark, A. E. Density Functional and Basis Set Dependence of Hydrated Ln(III) Properties. *J. Chem. Theory Comput.* **2008**, *4*, 708–718.
(10) Zhang, J.; Heinz, N.; Dolg, M. Understanding Lanthanoid(III) Hydration Structure and Kinetics by Insights from Energies and Wave Functions. *Inorg. Chem.* **2014**, *53*, 7700–7708.
(11) Zhang, J.; Dolg, M. Labile Capping Bonds in Lanthanide(III) Complexes: Shorter and Weaker. *J. Phys. Chem. A* **2015**, *119*, 774–780.
(12) Shiery, R. C.; Fulton, J. L.; Balasubramanian, M.; Nguyen, M.-T.; Lu, J.-B.; Li, J.; Rousseau, R.; Glezakou, V.-A.; Cantu, D. C. Coordination Sphere of Lanthanide Aqua Ions Resolved with Ab Initio Molecular Dynamics and X-Ray Absorption Spectroscopy. *Inorg. Chem.* **2021**, *60*, 3117–3130.
(13) Finney, A. R.; Lectez, S.; Freeman, C. L.; Harding, J. H.; Stackhouse, S. Ion Association in Lanthanide Chloride Solutions. *Chem. -Eur. J* **2019**, *25*, 8725–8740.
(14) Yazyev, O. V; Helm, L. Gadolinium (III) Ion in Liquid Water: Structure, Dynamics, and Magnetic Interactions from First Principles. *J. Chem. Phys.* **2007**, *127*, 84506.
(15) Ikeda, T.; Hirata, M.; Kimura, T. Hydration Structure of Y3+ and La3+ Compared: An Application of Metadynamics. *J. Chem. Phys.* **2005**, *122*, 244507.
(16) Kowall, T. H.; Foglia, F.; Helm, L.; Merbach, A. E. Molecular Dynamics Simulation Study of Lanthanide Ions Ln3+in Aqueous Solution Including Water Polarization. Change in Coordination Number from 9 to 8 along the Series. *J. Am. Chem. Soc.* **1995**, *117*, 3790–3799.
(17) Kowall, T.; Foglia, F.; Helm, L.; Merbach, A. E. Mechanisms of Water Exchange between Lanthanide(II) Aqua Ions [Ln(H 2O)n]3+ and Bulk Water: A Molecular Dynamics Simulation Approach Including High-Pressure Effects. *Chem. - A Eur. J.* **1996**, *2*, 285–294.
(18) Sessa, F.; Spezia, R.; D'Angelo, P. Lutetium(Iii) Aqua Ion: On the Dynamical Structure of the Heaviest Lanthanoid Hydration Complex. *J. Chem. Phys.* **2016**, *144*, 204505.
(19) Morales, N.; Galbis, E.; Martínez, J. M.; Pappalardo, R. R.; Sánchez Marcos, E. Identifying Coordination Geometries of Metal Aquaions in Water: Application to the Case of Lanthanoid and Actinoid Hydrates. *J. Phys. Chem. Lett.* **2016**, *7*, 4275–4280.
(20) Migliorati, V.; Serva, A.; Terenzio, F. M.; D'Angelo, P. Development of Lennard-Jones and Buckingham Potentials for Lanthanoid Ions in Water. *Inorg. Chem.* **2017**, *56*, 6214–6224.
(21) Qiao, B.; Skanthakumar, S.; Soderholm, L. Comparative CHARMM and AMOEBA Simulations of Lanthanide Hydration Energetics and Experimental Aqueous-Solution Structures. *J. Chem. Theory Comput.* **2018**, *14*, 1781–1790.
(22) Sessa, F.; D'Angelo, P.; Migliorati, V. Combined Distribution Functions: A Powerful Tool to Identify Cation Coordination Geometries in Liquid Systems. *Chem. Phys. Lett.* **2018**, *691*, 437–443.
(23) Floris, F. M.; Tani, A. A Study of Aqueous Solutions of Lanthanide Ions by Molecular Dynamics Simulation with Ab Initio Effective Pair Potentials. *J. Chem. Phys.* **2001**, *115*, 4750–4765.
(24) Clavaguéra, C.; Pollet, R.; Soudan, J. M.; Brenner, V.; Dognon, J. P. Molecular Dynamics Study of the Hydration of Lanthanum(III) and Europium(III) Including Many-Body Effects. *J. Phys. Chem. B* **2005**, *109*, 7614–7616.

(25) Duvail, M.; Spezia, R.; Vitorge, P. A Dynamic Model to Explain Hydration Behaviour along the Lanthanide Series. *ChemPhysChem* **2008**, *9*, 693–696.
(26) Duvail, M.; Vitorge, P.; Spezia, R. Building a Polarizable Pair Interaction Potential for Lanthanoids(III) in Liquid Water: A Molecular Dynamics Study of Structure and Dynamics of the Whole Series. *J. Chem. Phys.* **2009**, *130*.
(27) Duvail, M.; D'Angelo, P.; Gaigeot, M. P.; Vitorge, P.; Spezia, R. What First Principles Molecular Dynamics Can Tell Us about EXAFS Spectroscopy of Radioactive Heavy Metal Cations in Water. *Radiochim. Acta* **2009**, *97*, 339–346.
(28) Duvail, M.; Ruas, A.; Venault, L.; Moisy, P.; Guilbaud, P. Molecular Dynamics Studies of Concentrated Binary Aqueous Solutions of Lanthanide Salts: Structures and Exchange Dynamics. *Inorg. Chem* **2010**, *49*, 519–530.
(29) Marjolin, A.; Gourlaouen, C.; Clavaguera, C.; Ren, P. Y. Y.; Piquemal, J. P.; Dognon, J. P. Hydration Gibbs Free Energies of Open and Closed Shell Trivalent Lanthanide and Actinide Cations from Polarizable Molecular Dynamics. *J. Mol. Model* **2014**, *20*, 7.
(30) Li, P.; Song, L. F.; Merz, K. M. Parameterization of Highly Charged Metal Ions Using the 12-6-4 LJ-Type Nonbonded Model in Explicit Water. *J. Phys. Chem. B* **2015**, *119*, 883–895.
(31) Habenschuss, A.; Spedding, F. H. The Coordination (Hydration) of Rare Earth Ions in Aqueous Chloride Solutions from x-Ray Diffraction. II. LaCI3, PrCI3, and NdCI3. *J. Chem. Phys.* **1979**, *70*, 3758–3763.
(32) Habenschuss, A.; Spedding, F. H. The Coordination (Hydration) of Rare Earth Ions in Aqueous Chloride Solutions from x-Ray Diffraction. I. TbCI3, DyCI3, ErCI3, TmCI3, and LuCI3. *J. Chem. Phys.* **1979**, *70*, 2797–2806.
(33) Habenschuss, A.; Spedding, F. H. The Coordination (Hydration) of Rare Earth Ions in Aqueous Chloride Solutions from x-Ray Diffraction. III. SmCl3, EuCl3, and Series Behavior. *J. Chem. Phys.* **1980**, *73*, 442–450.
(34) Yamaguchi, T.; Nomura, M.; Wakita, H.; Ohtaki, H. An Extended X-Ray Absorption Fine Structure Study of Aqueous Rare Earth Perchlorate Solutions in Liquid and Glassy States. *J. Chem. Phys.* **1988**, *89*, 5153–5159.
(35) Allen, P. G.; Bucher, J. J.; Shuh, D. K.; Edelstein, N. M.; Craig, I. Coordination Chemistry of Trivalent Lanthanide and Actinide Ions in Dilute and Concentrated Chloride Solutions. *Inorg. Chem.* **2000**, *39*, 595–601.
(36) Persson, I.; D'Angelo, P.; De Panfilis, S.; Sandström, M.; Eriksson, L. Hydration of Lanthanoid(III) Ions in Aqueous Solution and Crystalline Hydrates Studied by EXAFS Spectroscopy and Crystallography: The Myth of the "Gadolinium Break." *Chem. - A Eur. J.* **2008**, *14*, 3056–3066.
(37) D'Angelo, P.; Zitolo, A.; Migliorati, V.; Chillemi, G.; Duvail, M.; Vitorge, P.; Abadie, S.; Spezia, R. Revised Ionic Radii of Lanthanoid(III) Ions in Aqueous Solution. *Inorg. Chem.* **2011**, *50*, 4572–4579.
(38) Näslund, J.; Lindqvist-Reis, P.; Persson, I.; Sandström, M. Steric Effects Control the Structure of the Solvated Lanthanum(III) Ion in Aqueous, Dimethyl Sulfoxide, and N,N'-Dimethylpropyleneurea Solution. An EXAFS and Large-Angle X-Ray Scattering Study. *Inorg. Chem.* **2000**, *39*, 4006–4011.
(39) Kofod, N.; Nawrocki, P.; Platas-Iglesias, C.; Sørensen, T. J. Electronic Structure of Ytterbium(III) Solvates—a Combined Spectroscopic and Theoretical Study. *Inorg. Chem.* **2021**, *60*, 7453–7464.

(40) Miyanaga, T.; Fujikawa, T. Quantum Statistical Approach to Debye-Waller Factor in EXAFS, EELS and ARXPS. II. Application to One-Dimensional Models. *J. Phys. Soc. Japan* **1994**, *63*, 1036–1052.
(41) Sawa, Y.; Miyanaga, T.; Tanida, H.; Watanabe, I. Temperature Dependence of EXAFS for Bromide Ions in Solution. *J. Chem. Soc. Faraday Trans.* **1995**, *91*, 4389–4393.
(42) Hoffmann, M. M.; Darab, J. G.; Palmer, B. J.; Fulton, J. L. A Transition in the Ni2+ Complex Structure from Six- to Four-Coordinate upon Formation of Ion Pair Species in Supercritical Water: An X-Ray Absorption Fine Structure, Near-Infrared, and Molecular Dynamics Study. *J. Phys. Chem. A* **1999**, *103*, 8471–8482.
(43) Fulton, J. L.; Hoffmann, M. M.; Darab, J. G. An X-Ray Absorption Fine Structure Study of Copper(I) Chloride Coordination Structure in Water up to 325°C. *Chem. Phys. Lett.* **2000**, *330*, 300–308.
(44) Simonet, V.; Calzavara, Y.; Hazemann, J. L.; Argoud, R.; Geaymond, O.; Raoux, D. Structure of Aqueous ZnBr2 Solution Probed by X-Ray Absorption Spectroscopy in Normal and Hydrothermal Conditions. *J. Chem. Phys.* **2002**, *116*, 2997–3006.
(45) Perdew, J. P.; Burke, K.; Ernzerhof, M. Generalized Gradient Approximation Made Simple. *Phys. Rev. Lett.* **1996**, *77*, 3865–3868.
(46) Hutter, J.; Iannuzzi, M.; Schiffmann, F.; VandeVondele, J. CP2k: Atomistic Simulations of Condensed Matter Systems. *Wiley Interdiscip. Rev. Comput. Mol. Sci.* **2014**, *4*, 15–25.
(47) VandeVondele, J.; Krack, M.; Mohamed, F.; Parrinello, M.; Chassaing, T.; Hutter, J.; Fast, Q. Fast and Accurate Density Functional Calculations Using a Mixed Gaussian and Plane Waves Approach. *Comput. Phys. Commun.* **2005**, *167*, 103–128.
(48) Goedecker, S.; Teter, M.; Hutter, J. Separable Dual-Space Gaussian Pseudopotentials. *Phys. Rev. B - Condens. Matter Mater. Phys* **1996**, No. 54, 1703–1710.
(49) VandeVondele, J.; Hutter, J. Gaussian Basis Sets for Accurate Calculations on Molecular Systems in Gas and Condensed Phases. *J. Chem. Phys.* **2007**, *127*, 114105.
(50) Lu, J. B.; Cantu, D. C.; Nguyen, M. T.; Li, J.; Glezakou, V. A.; Rousseau, R. Norm-Conserving Pseudopotentials and Basis Sets to Explore Lanthanide Chemistry in Complex Environments. *J. Chem. Theory Comput.* **2019**, *15*, 5987–5997.
(51) Lippert, G.; Hutter, J.; Parrinello, M. A Hybrid Gaussian and Plane Wave Density Functional Scheme. *Mol. Phys.* **1997**, *92*, 477–488.
(52) Grimme, S.; Antony, J.; Ehrlich, S.; Krieg, H. A Consistent and Accurate Ab Initio Parametrization of Density Functional Dispersion Correction (DFT-D) for the 94 Elements H-Pu. *J. Chem. Phys.* **2010**, *132*, 154104.
(53) Schenter, G. .; Fulton, J. L. XAFS Techniques for Catalysts, Nanomaterials and Surfaces; Iwasawa, I., Asakura, K., Tada, M., Eds.; Springer, 2017; pp 251–270.
(54) Ferrier, M. G.; Stein, B. W.; Batista, E. R.; Berg, J. M.; Birnbaum, E. R.; Engle, J. W.; John, K. D.; Kozimor, S. A.; Lezama Pacheco, J. S.; Redman, L. N. Synthesis and Characterization of the Actinium Aquo Ion. *ACS Cent. Sci.* **2017**, *3*, 176–185.
(55) Palmer, B. J.; Pfund, D. M.; Fulton, J. L. Direct Modeling of EXAFS Spectra from Molecular Dynamics Simulations. *J. Phys* **1996**, *100*, 13393–13398.
(56) Rehr, J. J.; Kas, J. J.; Prange, M. P.; Sorini, A. P.; Takimoto, Y.; Vila, F. Ab Initio Theory and Calculations of X-Ray Spectra. *C. R. Phys* **2009**, *10*, 548–559.
(57) Rousseau, R.; Schenter, G. K.; Fulton, J. L.; Linehan, J. C.; Engelhard, M. H.; Autrey, T. Defining Active Catalyst Structure and Reaction Pathways from Ab Initio Molecular Dynamics and Operando XAFS: Dehydrogenation of Dimethylaminoborane by Rhodium

Clusters. *J. Am. Chem. Soc.* **2009**, *131*, 10516–10524.
(58) Ravel, B.; Newville, M. ATHENA, ARTEMIS, HEPHAESTUS: Data Analysis for X-Ray Absorption Spectroscopy Using IFEFFIT. *J. Synchrotron Radiat.* **2005**, *12*, 537–541.
(59) Solera, J. A.; García, J.; Proietti, M. G. Multielectron Excitations at the L Edges in Rare-Earth Ionic Aqueous Solutions. *Phys. Rev. B* **1995**, *51*, 2678–2686.
(60) Helm, L.; Merbach, A. E. Water Exchange on Metal Ions: Experiments and Simulations. *Coord. Chem. Rev.* **1999**, *187*, 151–181.
(61) Fulton, J. L.; Bylaska, E. J.; Bogatko, S.; Balasubramanian, M.; Cauët, E.; Schenter, G. K.; Weare, J. H. Near-Quantitative Agreement of Model-Free DFT-MD Predictions with XAFS Observations of the Hydration Structure of Highly Charged Transition-Metal Ions. *J. Phys. Chem. Lett.* **2012**, *3*, 2588–2593.

For Table of Contents Only

TOC Graphic

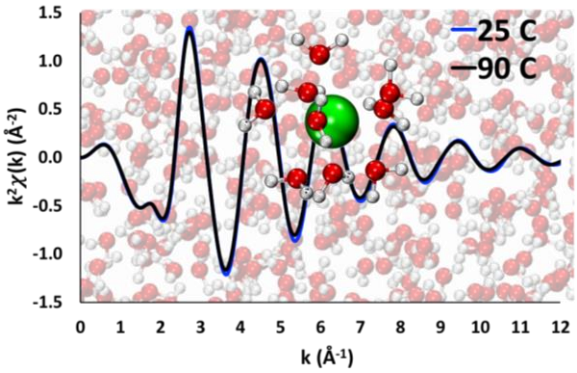

TOC Synopsis

In the liquid phase, temperature induces minor changes in the structure of the first coordination sphere of Ln^{3+} aqua ions.